New insight into naturally formed nanosilver particles: role of plant root exudates

Journal:	*Environmental Science: Nano*
Manuscript ID	EN-ART-11-2020-001188.R1
Article Type:	Paper

Environmental Significance Statement

Plant root exudates (RE) are abundant in terrestrial and aquatic environments, and can interact with Ag ions naturally present or accidentally/incidentally released into RE-rich environments. Currently, how RE modify the speciation and fate of Ag ions is poorly understood. This study is the first to demonstrate that RE fractions separated by molecular weight (MW) display different functions in the transformation of Ag^+ into Ag nanoparticles (nAg). In addition, a new theory was proposed to uncover the importance of Cl^- and biomolecules in RE in nAg formation. The new insights deepen our understanding of the cycling of Ag ions in agricultural and environmental systems, and will guide future assessment of their bioavailability and risk.

New insight into naturally formed nanosilver particles: role of plant root exudates

Huiyuan Guo,[‖,†] *Feng Han,*[#] *Heping Shang,*[†] *Sicheng Xiong,*[†] *My Huynh,*[†] *Lauren Thistle,*[†] *Liting Meng,*[†] *Lili He,*[‡,*] *Baoshan Xing*[†,*]

‖ Department of Chemistry, State University of New York at Binghamton, Binghamton, NY, 13902, USA

† Stockbridge School of Agriculture, University of Massachusetts, Amherst, MA 01003, USA

Key Laboratory of Subsurface Hydrology and Ecology in Arid Areas, Ministry of Education, Chang'an University, Xi'an, 710064, P. R. China

‡ Department of Food Science, University of Massachusetts, Amherst, MA 01003, USA

*Corresponding Authors

Dr. Baoshan Xing, Tel.: +1 413 545 5212; E-mail: bx@umass.edu

Dr. Lili He, Tel.: +1 413 545 5847; E-mail: lilihe@foodsci.umass.edu

Abstract

Manufactured silver nanoparticles (nAg) have been extensively studied because of questions and concerns on their unique properties, behavior and associated impacts on environmental health and safety. In contrast, naturally formed nAg, as one long-existing source of nanoparticles, have been less noticed and investigated. In this study, we evaluated the ability of natural ligands in plant root zone – root exudates (RE) – in transforming silver ions (Ag^+) to nAg and investigated the associated mechanism. We found that wheat RE had high reducing ability to convert Ag^+ to nAg under light exposure. A further test on molecular weight (MW)-based RE fractions showed that the photo-induced reduction of Ag^+ to nAg in pristine RE was mainly attributed to the 0-3 kDa fraction. Quantification of the silver species change over time suggested that Cl^- played an important role in photoconversion of Ag^+ to nAg through the formation and redox cycling of photoreactive AgCl. The accelerative function of AgCl as a photocatalyst was further demonstrated by the dramatically decreased generation of nAg in the dark. Potential electron donors for the photoreduction of Ag^+ were identified to be reducing sugars and organic acids of low MW. Meanwhile, the stabilization of the formed particles was controlled by both low (0-3 kDa) and high (>3 kDa) MW molecules. This study provides new insight into the formation mechanism of metal nanoparticles mediated by RE, which may further our understanding of the biogeochemical cycling and toxicity of heavy metal ions in agricultural and environmental systems.

1. Introduction

With accelerated commercialization and use of nanotechnology, the number of products containing nanomaterials is rising (http://nanodb.dk/en/). Engineered silver nanoparticles (nAg) are of wide commercial interest because of their superior properties and innovative features relative to their bulk counterparts. Their applications have been seen in a variety of fields, including textiles, biomedical use, environmental treatment, food packaging/food processing as well as surface plasmon resonance-based sensors. The wide applications of engineered nAg trigger curiosity in the public upon their environmental and biological behavior and impacts. If searching for "manufactured silver nanoparticles or engineered silver nanoparticles" and "environmental or biological behavior or impacts" through Web of Science (Nov 21, 2020), 5623 publications can be found. As a comparison, naturally occurring nAg, as another important source of nAg, have been less noticed and investigated, although their existence on earth is much longer than engineered nAg, and their environmental and biological impacts are largely unknown. When searching for "naturally occurring silver nanoparticles or naturally formed silver nanoparticles" and "environmental or biological behavior or impacts", only 80 articles showed up. The reason why they are less studied is probably that their source, formation pathways, and mechanisms in natural environments are not well understood. Without a good knowledge of where and how nAg is naturally formed, it is difficult to examine their fate, behavior, and bioavailability in the environment.

Based on the limited literature, naturally occurring nAg may be generated through three types of natural reducing ligands: natural organic matter (NOM),[1–3] microbial extracellular polymeric substances (EPS),[4] or biomolecules in plant tissues[5–7]. The mechanisms of NOM-induced reduction of silver ions (Ag^+) to nAg mainly involve oxygen-related reactive molecules,

such as superoxide ions[1] or ligand-to-metal charge transfer in photoactive complexes of Ag^+ and NOM[3]. A distinct mechanism was found on EPS-induced formation of nAg. Studies by Kang et al.[4] found that EPS secreted by bacteria could reduce Ag^+ to nAg (10-30 nm), leading to decreased bactericidal activity. The reduction of Ag^+ was mainly caused by hemiacetal groups of sugars in EPS. For plant-derived nAg, the formation was observed in plant roots, shoots[7,8] and even outside of plant roots/shoots[5,6,9]. However, the mechanisms have not been fully investigated. One group of researchers reported that when incubated in $AgNO_3$ solutions (0.05-1 mM), roots of intact plants of 16 species from 11 diverse families of angiosperms caused formation of Ag^0/Ag_2O nanoparticles (5-50 nm) outside of plant roots.[5] The mechanism they proposed is mainly due to the inherent reducing potential arising from plasma membrane bound dehydrogenases on root surface. However, a large knowledge gap exists on whether exudates released by plant roots can induce the natural formation of nAg. Root exudates (RE) are ubiquitous in the environment. Wherever there are plant roots growing, there are RE. The widespread existence of RE highlights the necessity to investigate whether and how RE modify the transformation and fate of Ag^+. Our group was among the first to demonstrate that live plant roots could induce the endogenous formation of nAg under sunlight irradiation.[10] In our previously published work, Ag^+ was exposed to live plant roots, which could interact with Ag^+ through different pathways. For example, plant roots could adsorb or absorb Ag^+, which altered its concentration in the plant root zone. Meanwhile, plant roots could release RE to react with Ag^+ externally. Plant roots-induced changes, including Ag^+ uptake and RE-induced transformation occurred at the same time in plant root zone, which made it difficult to identify the role of RE independently. Therefore, it is necessary to use isolated RE to investigate Ag^+ transformation caused by RE exclusively.

The objective of this study was to comprehensively unearth the role of plants-derived RE in transforming soluble Ag^+ to solid nAg and provide new insight on the formation mechanism of nAg in the presence of isolated RE. We observed the photoirradiation-promoted transformation of Ag^+ to nAg through characterizing the formed nAg and quantified the transformed silver species at different stages of the reaction. To uncover what RE molecules are responsible for the transformation, different RE fractions were separated based on molecular weight (MW) and interacted with Ag^+. Moreover, we performed an in-depth investigation on the possible mechanisms behind the photo-induced generation of nAg by RE. Based on several lines of evidence, a new theory for the natural formation of nAg was proposed to elucidate the functions of RE in the transformation.

2. Materials and Methods

2.1 Materials

Silver nitrate (ACS reagent, ≥99.0%), sodium chloride, superoxide dismutase (SOD), and methoxyamine hydrochloride were purchased from Sigma-Aldrich (St. Louis, MO). Triton™ X-114, sodium thiosulfate, nitric acid (70%), and ferbam were used as obtained from Fisher Scientific (Pittsburgh, PA). N-Methyl-N-(trimethylsilyl) trifluoroacetamide (MSTFA) was ordered from Acros Organics (Geel, Belgium). Wheat seeds were obtained from Johnny's Selected Seeds. Milli-Q water (18 MΩ·cm) was used to prepare all reagent solutions unless indicated otherwise.

2.2 Methods

2.2.1 Collection and characterization of RE

The wheat seeds were grown in moisturized vermiculite and cultivated for 7 days in a greenhouse (22-20 °C/16 h light, 18-20 °C/8 h dark). Afterwards, the roots of the wheat seedlings

were gently cleaned with Milli-Q water. To collect RE, the clean roots of 15 intact seedlings were soaked in a 40 mL Milli-Q water-filled glass bottle, which were wrapped in aluminum foil to protect the roots from light. After 24 hours, RE were collected and filtered through 0.45 μm membrane (Nitrocellulose membrane, Millipore) to remove small root debris. After filtration, RE were stored at -20 °C until use.

We first characterized the collected RE using multiple techniques. The pH of RE was measured to be 6.7 ± 0.1 by a pH meter (Fisher Scientific, XL200). We also quantified the concentration of chloride ions (Cl^-) in RE using ion chromatography (Metrohm 850 Professional IC), which showed a value of 0.33 ± 0.003 mM. To analyze the quantity and speciation of organic components in RE, the collected RE were subjected to total organic carbon content (TOC) (Shimadzu, TOC-L) and GC-MS (Shimadzu, GCMS-QP2010 Ultra) analyses. Total organic carbon (TOC) was found to be 125 ± 3 mg/L. GC-MS sample derivation and measurement were performed by following a protocol by Lisec et al.[11] Briefly, a lyophilized 3 ml RE was derivatized by 160 μL of methoxyamine hydrochloride (20 mg/mL in pyridine, 2 h, 37˚C) and 280 μL N-methyl-N-(trimethylsilyl) trifluoroacetamide (MSTFA) (30 min, 37˚C). The injection volume was 1 μL. An injector in a splitless mode was used. The GC separation was conducted utilizing an SH-Rxi-5ms Capillary Column (30 m, 0.25 μm, 0.25 mm, Shimadzu, USA). The temperatures of injection, interface and ion-source were set as 230, 250 and 210˚C, respectively. The gas flowed at a rate of 1 μL/min. The column temperature was programmed to be 1 min at 70˚C, 6 min ramp to 76˚C, 50 min ramp to 330˚C, 10 min at 330˚C. The column end was connected with an ion trap mass spectrometer, which recorded mass spectra at a speed of 2 scans/s in a range of m/z 50-600. The mass spectra were interpreted through similarity searches in the NIST public database.

2.2.2 Reaction of RE with Ag^+

The collected RE interacted with $AgNO_3$ in a chamber room equipped with two visible light lamps (40 Watt, F40CW, Philips) at room temperature. The light intensity was set as 8288 ± 103 lux, unless otherwise noted. Before light exposure, RE were mixed with Ag solutions at a variety of environmentally relevant concentrations (0.05 mM-1 mM, i.e., 5.4-107.9 mg/L). The Ag concentration range in soils/sediments was reported to be from 0.01-1000 mg/kg (9.27×10^{-5}–9.27 mM).[12,13] In natural surface water, the Ag levels typically range from ng/L to μg/L.[13] However, the Ag concentration in surface water can be high in the mg/L level if contaminated by municipal and industrial wastewater effluents, mining drainage, or leaching from soils/sediments.[14,15] All the Ag^+ transformation experiments were carried out in replicate with different time intervals (0-12 h unless otherwise noted). Control experiments were conducted in the dark with vials covered by 3 layers of aluminum foil.

2.2.3 Characterization of the formed nAg in RE

The formation of nAg was monitored by a UV-Vis spectrophotometer (Agilent 8453). Meanwhile, the zeta potential of the formed particles was measured by dynamic light scattering (DLS, Brookhaven, 90Plus). Particle X-ray powder diffraction (XRD) patterns were obtained using a PANalytical X'Pert diffractometer. The morphology, structure and speciation of the formed nanoparticles were characterized by scanning electron microscopy (SEM, FEI Magellan 400 XHR) with energy dispersive X-ray spectroscopy (EDS, Oxford 80 mm^2 X-Max). The crystal structure of nAg was measured by high-resolution TEM (HRTEM) (JEOL, JEM-2200FS, Japan) with selected area electron diffraction (SAED). Details on the sample preparation for SEM-EDS and HRTEM-SAED were provided in SI (section 1).

Raman spectroscopy and Fourier-transform infrared spectroscopy (FTIR) were used to characterize the surface chemistry of the formed particles. The formation of nAg in RE was confirmed by a previously established surface-enhanced Raman spectroscopy (SERS) method[16] with minor modification. Briefly, by using ferbam as an indicator molecule, the formation of nAg is readily indicated by the enhanced signals of ferbam. The experimental procedure and settings of the Raman spectroscopy and FTIR are presented in SI (section 2).

2.2.4 Quantification of the Ag species over time

The Ag species during the transformation were quantified using inductively coupled plasma-mass spectrometry (ICP-MS 2030, Shimadzu). Based on the characterization data (Figure 1), two types of Ag-containing particles (AgCl and nAg) were identified. In case the transformation did not consume all Ag^+, we also measured Ag^+ in the samples. In order to separate three Ag species (AgCl, nAg and Ag^+), a selective centrifugation-dissolution-centrifugation method developed by Ying et al.[17] was used with minor modification. In brief, Ag^+ was isolated from the formed particles through high-speed centrifugation (13,500 rpm, 30 min). The supernatant, which contains Ag^+, was collected and labelled as S1. The particle precipitates were re-suspended in a solution of 0.1% (w/v) Triton X-114 and 20 mM $Na_2S_2O_3$ prior to the second cycle of centrifugation. Triton X-114 functioned as a stabilizing agent to protect nAg. $Na_2S_2O_3$ was used to dissolve AgCl particles. After the second cycle of centrifugation (13,500 rpm, 30 min), the dissolved Ag^+ from AgCl stayed in the supernatant (S2) and was isolated from nAg in the precipitates (P). Prior to ICP-MS analysis, P was digested by concentrated nitric acid (0.5 mL) and diluted using Milli-Q water while S1 and S2 were diluted by nitric acid (3%). After obtaining the Ag content in S1, S2 and P, a summary of Ag in the three fractions was calculated to represent the

total Ag content. The reliability of the method was tested with amended control samples and the recovery rates were 106.5 ± 2.9% for AgCl (0.33 mM) and 89.8 ± 3.5% for nAg (60 nm, 10 mg/L).

2.2.5 Mechanistic studies on the RE-induced formation of nAg

To reveal the mechanism underlying the RE-induced formation of nAg, we investigated the transformation of Ag^+ to nAg mediated by different fractions of RE. RE were fractioned into two parts (0-3 kDa and >3 kDa) by using ultra-centrifugal filter membranes (3 kDa, Amicon Ultra-15, Millipore). Before RE fraction, the ultra-centrifugal filters were centrifuged twice with 15 mL Milli-Q water to remove glycerol. After cleaning, pristine RE (15 mL) was centrifuged in a 3 kDa filter. The retentate was collected as RE (> 3 kDa) while the filtrate was regarded as RE (0-3 kDa). The centrifugation time and speed were adjusted according to the filter device user guide to ensure a final retentate volume of ~2% of initial volume. The collected retentate was filled up to match the initial volume (15 mL). Different fractions of RE were compared with pristine RE regarding their ability to reduce Ag^+.

We also investigated the transformation of Ag^+ under light irradiation in the presence of RE with addition or removal of Cl^- in RE. By mixing additional Cl^- (0.33 mM) with RE, the original Cl^- concentration was doubled. The removal experiment was carried out by providing excessive Ag^+ (1 mM) to react with Cl^- so that free Cl^- are transformed to AgCl particles, which can be removed by filtration through a ultra-centrifugal filter membrane with a pore size of ~3 nm (100 kDa, Amicon Ultra-15, Millipore).

To further our understanding of the RE-induced formation of nAg, we examined the previous studies on naturally formed nAg,[1–3,5]. Accordingly, three possible reducing sources were tested: 1) proteins (e.g., enzymes)[5], 2) reactive transients (e.g., superoxide),[1,2] and 3) electron

shuttling within Ag^+-organic complexes[3]. In order to demonstrate how proteins in RE affect the nAg formation, RE were boiled in a 100 °C water bath for 20 minutes. After the boiled RE cooled down, its ability to transform Ag^+ (1 mM) was compared with pristine RE. Meanwhile, we determined the protein content in RE by using a method reported by Scopes.[18] Briefly, the pristine RE was analyzed by UV-Vis spectroscopy using a 1-cm quartz cell in a wavelength range of 190-1100 nm. The protein concentration was calculated based on the following equations:

$$\varepsilon_{205}^{1\ \mathrm{mg/mL}} = 27 + 120 \times (A_{280}/A_{205}) \qquad \text{Equation 1}$$

$$A_{205} = \varepsilon_{205}^{1\ \mathrm{mg/mL}}\, cl \qquad \text{Equation 2}$$

where A_{280} and A_{205} represent the UV-Vis absorbance at 280 nm and 205 nm, respectively. The $\varepsilon_{205}^{1\ \mathrm{mg/mL}}$ is the absorptivity coefficient with unit of $(mg/mL)^{-1}\ cm^{-1}$, c is the estimated protein concentration, and l is path length, which is 1 cm here.

To figure out if reactive transients are responsible for Ag^+ photoreduction, two strategies were used. First, we purged RE with pure nitrogen for 1 hour to remove the precursor of reactive transients—dissolved O_2—prior to interacting with Ag^+ while another group was purged with air for 1 hour to increase the dissolved O_2. Second, we removed superoxide radical in RE by adding SOD (150 U/mL and 600 U/mL) into the reaction solution.[1] To test if the formation of nAg is a result of electron shuttling within Ag^+-organic complexes, $NaNO_3$ (0 mM, 5 mM and 10 mM) was added to compete with Ag^+ to bind with organic molecules in RE.[3]

3. Results and discussion

3.1 Characterization of the formed nAg

To examine if RE can induce the transformation of Ag^+ to nAg, we incubated RE with Ag^+ and monitored the change over time. As seen in Figure 1a, the Ag^+-RE mixture displayed an evident color evolution from colorless to light brown then to dark brown over the 8-h light irradiation. The dark brown color stabilized from 8 h to 12 h with precipitates observed at 12 h. The corresponding UV-Vis spectra were recorded with an absorbance peak occurring at 450 nm, indicating the formation of nAg (Figure 1b). This peak increased from 0 to 8 h and slowed down from 8 h to 12 h (Figure 1c), which is consistent with the color change trend (Figure 1a). A plot based on the UV-Vis absorbance of nAg shows that the formation kinetics followed a pseudo-first-order reaction (Figure S1)[19]:

$$-Ln[(A_{max} - A_t)/A_{max}] = kt$$

where A_{max} and A_t are the absorbance of nAg at 450 nm at time max and time t. Based on Lambert-Beer's law, the nAg concentration is positively related to the UV-Vis absorbance.[20] Therefore, A_{max} and A_t were used to calculate the nAg formation kinetics, which shows a rate constant of k=0.3466 h^{-1} (R^2=0.9989) (Figure S1).

The formation of nAg was further supported by a SERS method. This method relies on nAg-specific Raman enhancement of an indicator, which is induced by a unique property of nAg – surface plasmon resonance.[21,22] Compared with the Raman spectrum of the indicator alone (i.e., ferbam), the one with RE-induced particles exhibited much higher Raman signal intensity (Figure S2). The nAg-specific enhancement of the indicator Raman signals confirms the formation of nAg in RE. Further, the formed nAg were characterized by HRTEM-SAED (Figure S3). The d-spacings

were determined to be 2.32 ± 0.02 Å and 2.04 ± 0.05 Å, which are the features of the (111) and (200) lattice planes of Ag(0), respectively.[1,3,23–25] The size distribution of the formed particles was characterized by TEM and analyzed by ImageJ, showing a size increase from 48 to 103 nm over 12 h (Figure S4). The precipitation of the formed particles observed at 12 h (Figure 1) may be caused by particle size increase. It is also possible that the particle instability was due to the surface charge decline as indicated by the zeta potential data (Figure S5).

In order to characterize the surface chemistry of the formed particles, analyses by both FTIR and Raman spectroscopy were performed. FTIR spectra for samples at 0 h and 12 h are shown in Figure S6. Six prominent peaks are observed at 3342, 2928, 1654, 1540, 1388, and 1068 cm^{-1}, which can be assigned to O-H stretching, C-H stretching in $-CH_3$ and $-CH_2-$, C=O stretching, N-H bending or OCO stretching, OCO stretching, and C-O stretching, respectively.[26,27] The associated molecules are likely to be amino acid-based molecules (amino acids, peptides and proteins), carboxylic acids, sugars, and alcohols.[26,27] As for Raman spectra (Figure S7), the signal intensity and number of the surface molecules on the formed particles increased from 0 h to 12 h. The increased Raman enhancement is likely due to the particle size increase from 48 nm to 103 nm (Figure S4) or particle concentration increase (Figure 1 and 2).[16] By analyzing the functional groups associated with Raman peaks (Figure S7), we were able to identify the biomolecules on the particle surface. First, it was noticed that three peaks occurred at similar positions as those in FTIR spectra, 2790, 1599, and 1391 cm^{-1}, which are attributed to C-H stretching in $-CH_3$ and $-CH_2-$, OCO stretching, and OCO stretching, respectively.[26,27] The Raman peaks observed at 1000 and 1044 cm^{-1} were due to ring breathing mode and C-O stretching, respectively.[26,27] The weak peaks at 870 and 805 cm^{-1} correspond to C-C-N stretching, and C-C-O stretching, respectively.[26,27] The strongest peak at 233 cm^{-1} is ascribed to Ag-Cl vibration, implying the interaction between the

particle surface and Cl^-.[28,29] The Raman spectra indicate that the biomolecules on the formed particle surface might contain amino acid-based molecules (amino acids, peptides and proteins), carboxylic acids, sugars, and alcohols,[26,27] which is in agreement with FTIR data. Meanwhile, as shown above, Raman data also provide clues on the particle size, concentration as well as interaction with Cl^-.

3.2 Quantification of silver species during transformation

To quantitatively determine the transformation products, we measured the amount of each Ag species (Ag^+, nAg and AgCl) at different time points using ICP-MS. In addition to nAg, AgCl was included as one of the potential transformation products because Ag-Cl interaction was observed by Raman spectroscopy. As noted in Figure 2, the total Ag concentration stayed at ~1.04 mM consistently over time, which agreed well with what we added initially (1 mM), manifesting that our detection method was reliable with good Ag recovery. Also, we found that [Ag^+] decreased and [nAg] increased over time, showing that Ag^+ was gradually transformed to nAg. Interestingly, the Ag levels in AgCl remained constant from 0 h to12 h. Based on the ion chromatography measurement, RE contained 0.33 ± 0.0031 mM Cl^-. The presence of AgCl at 0 h is because when Ag^+ was in contact with RE, AgCl formed immediately. This is also reflected by the appearance of a UV-Vis absorbance peak at 260 nm in the beginning of the reaction (Figure 1), which is representative of AgCl according to the literature.[30–32] In addition, we observed cubic particles in the transformed samples through SEM images, which were confirmed to be AgCl by EDS analysis (Figure S8).

3.3 Mechanisms of RE-induced nAg formation

3.3.1 Formation of nAg by molecular weight (MW)-based RE fractions

To figure out the reducing sources in RE that are responsible for the transformation of Ag^+, we separated RE into two fractions based on MW (0-3 kDa and >3 kDa) using ultracentrifugation filter tubes. After separation, each fraction interacted with Ag^+ (1 mM) under light irradiation. As shown in the UV-Vis spectra (Figure 3a and 3b), the 0-3 kDa fraction of RE led to a significant absorbance elevation from 0 h to 4 h while the >3 kDa fraction only induced slight peak increase. The nAg formation kinetics by the two fractions was compared with that by pristine RE. Initial formation rate (r) of nAg, which has been adopted in previous studies to indicate the reducing ability of NOM,[1,33] was calculated as the slope of a linear curve plotted based on the change of UV-Vis absorbance at 450 nm as a function of time over 1 h. As noted in Figure 3e, the initial formation rates were similar between pristine RE (r=0.5511 min^{-1}) and the 0-3 kDa fraction (r=0.5486 min^{-1}), both of which were largely higher than that by the >3 kDa fraction (r=0.0045 min^{-1}), indicating that the 0-3 kDa fraction rather than the >3 kDa plays a major part in inducing nAg generation. In addition to the UV-Vis absorbance peak of nAg at 450 nm, the pristine RE and the 0-3 kDa fraction shared another peak at 260 nm (Figure 3a), which is a characteristic band of AgCl particles.[30–32] The co-presence of AgCl and nAg peaks in the 0-3 kDa fraction and pristine RE suggests that Cl^- in the 0-3 kDa fraction might be involved in the nAg formation.

As mentioned above, the >3 kDa fraction was less effective in inducing nAg formation compared with the 0-3 kDa fraction or pristine RE (Figure 3e). To test if this is caused by the lack of Cl^-, we added Cl^- into the >3 kDa fraction at a concentration equivalent to that (0.33 mM) in pristine RE or the 0-3 kDa fraction. In the beginning, the UV-Vis absorbance increased more quickly (Figure 3c) than the group without Cl^- addition (Figure 3b). Meanwhile, due to the addition

of Cl^-, the UV-Vis peaks were broader and decreased after 1h, indicating the formed larger particles are unstable. As shown in Figure 3d, the particles formed by the group of >3 kDa RE with Cl^- addition precipitated readily, showing weaker stability than those in pristine RE. Therefore, adding Cl^- into the >3 kDa fraction triggered faster generation of Ag-containing particles, but the produced particles were not as stable as those in pristine RE or the 0-3 kDa fraction. This result shows that to form stable nAg, molecules in the 0-3 kDa fraction other than Cl^- are also needed. In addition, we noticed that the formation dynamics at a later stage (4-8 h) was distinct between pristine RE and the 0-3 kDa fraction. Particularly, at 8 h both AgCl and nAg peaks became broader and lower in the 0-3 kDa fraction (Figure 3a) while in pristine RE these two peaks increased (Figure 1b). The broadening and decreasing trend of the AgCl and nAg peaks in the 0-3 kDa fraction could be caused by aggregation and aging of the formed particles, indicating that without MW >3 kDa molecules, the formed particles were less stable. Taken together, the stability of the formed particles was compromised without either the >3 kDa or the 0-3 kDa fraction, suggesting the stabilizing effects of molecules in both fractions.

3.3.2 The function of Cl^- in RE

To further demonstrate the function of Cl^- in RE-induced formation of nAg, we modified RE by adding external Cl^- (Figure 4a) or removing original Cl^- in RE (Figure 4b) before incubation with Ag^+ under light irradiation. The reduction of Ag^+ was enhanced by around two folds when 0.33 mM Cl^- was added into RE (Figure 4d). The added Cl^- concentration was equivalent to that in RE and therefore doubled the total Cl^- amount. The increased Cl^- concentration resulted in higher concentration of AgCl, which accelerated the transformation of Ag^+ under light exposure. On the other hand, the removal of Cl^- in RE decreased the formation rate of nAg dramatically, suggesting that RE without Cl^- could not induce significant reduction of Ag^+ to nAg (Figure 4d).

One possible explanation for the enhanced nAg formation by AgCl is that AgCl provides a solid surface where Ag atoms could accumulate and form nAg. The transformation of a silver ion to a single silver atom is endergonic (-1.8 V). As such, the formation of Ag atom is thermodynamically unfavorable relative to Ag^+/e^-. However, the redox potential of Ag^+ turns exergonic (+0.8 V) on the surface of aggregated silver atoms. It has been reported that Ag^+ alone could not be reduced by NOM or peptides, but with the assistance of AgO[1] or AgCl nucleus[17,34], the reduction became thermodynamically feasible. To test if this is the reason why AgCl enables faster formation of nAg in RE, we used citrate-nAg (60 nm, 1 mg/L) as a substitute of aggregated Ag atoms in AgCl. Before mixing RE with Ag^+, Cl^- was removed to prevent the formation of AgCl. As Figure 4c indicates, the group with added nAg had similar reaction rate to the group without addition, both of which were lower than that with pristine RE, suggesting that the pre-added silver nanoseeds did not facilitate nAg formation under light exposure. Hence, the accelerative role of AgCl in nAg formation is mainly attributed to other mechanisms.

AgCl is a semiconductor that produces excited electrons and holes upon irradiation by high-energy light. The band gap energy of AgCl is ~3.3 eV (~380 nm).[35,36] When the irradiation energy is equivalent or higher than the band gap energy of AgCl, an electron (e^-) is excited from the valence band to the conduction band, leaving a hole (h^+) generated in the valence band. The excited electrons have the potential to reduce Ag^+ to nAg. In this study, visible light (400 nm-700 nm) was used as the irradiation source, which has photon energy lower than 3.3 eV and is thus inefficient in exciting electrons in AgCl. However, this situation was changed when there were nAg pre-formed in the solution. As observed in Figure 4b, nAg were able to be formed slowly in RE without AgCl photocatalysis, leading to the copresence of nAg and AgCl. The mixture of nAg/AgCl was known as a photocatalyst that is photoreactive upon visible light irradiation because

metallic silver nanoparticles exhibit localized surface plasmon resonance (LSPR) in visible light range.[37–39] It has been reported that nAg/AgCl as photocatalysts are advantageous than AgCl alone because nAg act as electron sinks and enable the separation of photogenerated electrons and holes;[39] and the visible light absorption by nAg improves the photocatalytic efficiency of the combined photocatalyst under visible light irradiation.[37,40] This explains why nAg were quickly generated in RE under visible light irradiation.

Previous studies have shown that photoirradiation of AgCl could lead to the formation of nAg on the surface of AgCl.[41–43] In these studies, the ratio of Ag/Cl was either 1 or less than 1, which means limited amount of Ag^+ was available in the solution and the reduction occurred on the surface of AgCl. AgCl was reported to degrade to Ag (0) and Cl_2 under strong light irradiation.[10,43,44] However, in this study we found AgCl concentration remained constant. When Ag^+ (1 mM) are exposed to RE, the Cl^- (0.33 ± 0.0031 mM) in RE can react with part of Ag^+ to form AgCl because of its low solubility product (Ksp=1.77×10^{-10}). As the ratio of Ag/Cl (~3) was larger than 1, free Ag^+ was redundant in the solution. We found that nAg were formed under visible light irradiation without the consumption of AgCl. The constant quantity of AgCl during the reaction and the photoreactive property of AgCl imply that AgCl, with the assistance of nAg, may serve as a photocatalyst and be regenerated through redox cycling. It is likely that the photoexcited electrons produced by nAg/AgCl reduce free Ag^+ in the solution to nAg while generating Cl_2. As a strong oxidant, Cl_2 can react with electron donors (e.g., reducing sugars and organic acids) in RE to produce Cl^-. When the formed Cl^- is in contact with free Ag^+, AgCl is regenerated and can continuously acts as a photocatalyst to reduce Ag^+ to nAg. Liu et al. examined the formation of nAg by NOM as influenced the Cl^-.[45] The Cl^- concentration range they used (0-1 mg/L) is much lower than what we observed in RE (0.33 mM=11.7 mg/L). Although they noticed that the

formation of nAg was inhibited after removing Cl^- from NOM, they did not ascribe the photocatalytic function of AgCl as a potential contributor to the nAg formation. Another research group discovered that 100 mg/L Cl^- can increase the reduction of Ag^+ (10 mg/L) in the presence of NOM either at 25 °C or after freeze-thaw cycles in the dark.[46] However, the reduction mechanism was not defined in that study. It is highly possible that the presence of Cl^- in NOM solution enables the reduction of Ag^+ through the photocatalysis by nAg/AgCl. Future efforts are required to examine if a similar mechanism contributes to the enhancing effect of Cl^- on Ag^+ transformation by NOM.

3.3.3 The role of organic molecules in RE

In addition to light condition, we further investigated the transformation of Ag^+ by RE in the dark. As light is required for photocatalysis, using the dark condition herein could exclude the photocatalytic function and help us map out components other than Cl^- in RE that contributes to nAg formation. Based on our UV-Vis spectroscopic measurements in Figure 5a, the absorbance peak of nAg became gradually noticeable over time (0-261 h) under dark condition. However, even at 261 h, the nAg formed in the dark were lower than those formed at 8 h (Figure 1) under photoirradiation, showing that the generation of nAg is feasible in the dark but much slower. Obviously, it was the photocatalysis induced by light irradiation that caused the difference. In our published work involving Ag^+ transformation by live plant roots,[10] the nAg formation in the dark was not observed, which may be caused by the uptake of free Ag^+ by live plant roots that limited its availability. Herein, we used isolated RE to exclude root uptake and are the first group to report RE-induced formation of nAg in the dark. We sought to figure out what biomolecules in RE contributed to this process. In this study, the UV-Vis spectrum of RE itself exhibits a high absorbance at ~280 nm (Figure S9), indicating that amino acids-containing biomolecules exist in

RE.[47] RE are known to contain different types of proteins, including enzymes.[48–50] Based on the UV-Vis absorbance (Figure S9), the protein content was estimated to be 19.8 mg/L (calculation details shown in Methods). To test how proteins in RE affect nAg formation, boiling was used to deactivate them. The deactivation gave rise to significantly slower formation of nAg in the dark (Figure 5b and 5c), suggesting that the proteins in RE were involved in nAg formation in the dark. In agreement with our finding, prior studies reported that proteins can mediate the synthesis of nAg without the assistance of light.[47,51–53] We made further efforts to investigate if proteins can impact the photoconversion of Ag^+ to nAg. The data (Figure S10) demonstrates a slight decline of initial nAg formation rate induced by boiled RE under photoirradiation, suggesting that proteins plays a minor role in nAg photogeneration. Therefore, it is expected that organic molecules other than proteins are the major electron donors for Ag^+ photoreduction. To analyze organic molecules in RE, GC-MS was used (Figure S11), which showed that RE contain a variety of sugars and organic acids, including reducing sugars and organic acids, such as D-fructose, D-mannose, α-D-lactose, and lactic acid. These types of molecules have been used as reducing agents to synthesize metal nanoparticles.[54–56] Based on the aforementioned fact that the RE fraction of low MW molecules (0-3 kDa) induced similar initial formation rate of nAg to that of pristine RE under light irradiation (Figure 3a), it is highly possible that sugar and/or organic acids of low MW (0-3 kDa) in RE are the major electron donors for the light-induced transformation of Ag^+ to nAg.

3.3.4 Impacts of superoxide radical and ligand-to-metal charge transfer

Previously, light-driven formation of nAg was reported in natural organic matters (NOM)-rich environments.[1,3] The mechanism lies in photo-induced generation of superoxide radical ($O_2^{\bullet-}$)[1] or ligand-to-metal charge transfer (LMCT) in photoactive complexes of Ag^+ and NOM[3]. To examine if $O_2^{\bullet-}$ is involved in the photoreduction of Ag^+ by plant RE, we purged RE with N_2 or air

in order to change the level of dissolved O_2 (Figure S12a), which is a required component for $O_2^{\bullet-}$ generation.[1] Comparisons on sample colors and UV-Vis spectra showed that the formation of nAg was independent from dissolved O_2 level, indicating that oxygen-derived reactive species, including $O_2^{\bullet-}$, are not responsible for Ag^+ photoreduction. The irrelevance of $O_2^{\bullet-}$ with RE-induced nAg formation was further confirmed by using SOD as a $O_2^{\bullet-}$ scavenger (Figure S12b). We found that the initial formation rate of nAg was not inhibited by the presence of SOD, indicating that $O_2^{\bullet-}$ is not a contributor to the RE-mediated Ag^+ photoreduction. The slightly lower absorbance from 2 h to 8 h for the groups containing SOD may be caused by the peak shape change induced by the stabilizing effect of SOD.[57,58]

Hou et al. reported that sunlight could significantly accelerate the formation of AgNPs through enhancing LMCT in photoactive complexes of Ag^+ and NOM.[59] To examine the LMCT pathway, they added competing cations (Na^+) into NOM, which decreased the formation of nAg. We performed a similar experiment using RE with results (Figure S13) showing that Na^+ did not affect the initial reaction rate but rather resulted in the particle aggregation at a later stage because of the high ionic strength.[60–62] As such, the LMCT pathway did not contribute to Ag^+ reduction.

3.3.5 Proposed mechanism

Based on all the above findings, we propose the following mechanism to explain the RE-induced formation of nAg (Figure 6): The biomolecules in RE, especially those of low MW (0-3 kDa), provide electrons for nAg generation. Also, biomolecules in both the 0-3 kDa and >3 kDa fractions act as stabilizing agents for the formed particles. The presence of Cl^- in RE enhances the photo-transformation of Ag^+ to nAg through the catalytic role of nAg/AgCl in accelerating the reduction of Ag^+ by biomolecules in RE. When Ag^+ are released into RE, part of them are converted to AgCl by reaction with Cl^- in RE. In the dark, the formation of nAg occurs at a slow

pace via the reduction of Ag^+ by biomolecules in RE, such as proteins (Figure 5 and Figure 6). Under light irradiation, nAg is formed quickly due to the reduction by photoexcited electrons from nAg/AgCl. Meanwhile, Cl_2 is produced from the oxidation of AgCl by the left oxidative holes. When Cl_2 is in contact with water, Cl^-, HClO and ClO^- are generated.[39] HClO and ClO^- can be further converted to Cl^- due to their strong oxidative capacities, especially in the presence of reducing biomolecules (e.g., reducing sugars and organic acids) in RE.[63–65] Meanwhile, Cl_2 may directly interact with reducing biomolecules and be reduced to Cl^-.[38,43] The resulting Cl^- binds with redundant Ag^+ in the solution to regenerate AgCl, which continuously act as a photocatalyst to reduce Ag^+ to nAg. In summary, the occurrence of Cl^- in RE facilitates the electron transfer between Ag^+ and biomolecules in RE through photocatalytic activity of nAg/AgCl. In this study, we were unable to measure reactive chlorine species, including Cl_2, HClO and ClO^- due to their rapid transformation into Cl^-, which reacted with free Ag^+ quickly to form AgCl in the system. A recent study investigating the influence of Cl^- on NOM-induced nAg formation found the measurement of reactive chlorine species was challenging as well.[66]

In the present work, we studied the natural formation of nAg by RE in both dark and visible light condition. In the real world, light can penetrate the top layer (0.2-0.4 mm) of the soil.[67] RE-induced nAg formation is likely to proceed faster on the top layer due to photocatalysis. Since RE are also present in surface waters, which are exposed to light in a deeper level (e.g., 4-18 m in lakes[68]), light-accelerated generation of nAg is expected in surface waters. Even in the dark, RE are redox reactive and enable the relatively slow formation of nAg through reducing biomolecules. As such, our work provides new and fundamental knowledge on the speciation and fate of Ag^+ upon exposure to RE in both dark and light environments.

We notice that in previous studies that examined the transformation of Ag^+ to nAg by plant tissues, NOM, and microbial extracellular polymeric substances (EPS), a commonly used initial concentration of Ag^+ is ~1 mM (ca. 107.9 ppm) or a value of similar magnitude.[5,59,69,70] In order to compare our results with the previous studies, we utilized a similar level of Ag^+. These studies along with the current one have important implications for environmental systems contaminated by high concentrations of Ag^+, such as wastewater effluents, mining drainage, or soil/sediment leaching. It was reported that 150 ppm Ag^+ were detected in Genesee River (USA) sediments, the recipient of photographic manufacturing wastes.[14] High concentration of Ag^+ (e.g., 31 ppm) can also be present in some soils (e.g., Idaho, USA).[15] In addition to simulating scenarios with high levels of Ag^+ contamination, we also tested a range of lower concentrations (0.05-0.33 mM). The results show that nAg could also be formed when low levels of Ag^+ were in contact with RE (Figure S14). Because RE are widely distributed in both natural and man-made environments, RE-induced formation of nAg is an important process that affects the environmental behavior and fate of Ag^+.

The uniqueness of this study is that we provide new and in-depth insight into natural formation of nAg through Ag^+ transformation induced by key components in a widespread natural ligand – RE. Similar to engineered nAg, naturally formed ones have the potential to be transformed into other species, such as Ag^+, AgS, and AgCl, by natural processes or anthropogenic activities.[46,71,72] On the other hand, prior work demonstrated that nAg can be regenerated from Ag^+, AgCl or AgS under certain circumstances.[17,43,44,73] However, the importance of RE shown in this study calls for future work to consider the influence of RE on the transformations between nAg and other silver species, and the associated environmental and biological implications.

4. Conclusions

In this study, we investigated how plant RE affected the transformation and speciation of Ag^+. We are among the first to discover that different fractions of RE (MW-based) play distinct roles in nAg formation. We identified that the 0-3 kDa RE fraction was a major contributor to photo-induced formation of nAg. Specifically, Cl^- in the 0-3 kDa fraction could react with Ag^+ to generate photoreactive AgCl which provided electrons for the reduction of Ag^+. Meanwhile, small biomolecules including reducing acids and sugars acted as electron donors to facilitate the regeneration/recycling of AgCl, which existed constantly in the system and catalyzed the reduction of Ag^+. Cl^- and biomolecules in RE are ubiquitous elements in aquatic and soil systems. It is of significance to investigate how they affect the transformation of Ag^+ to nAg in RE-rich environments. This study demonstrates that plant RE provide a new driving force for the photogeneration of naturally occurring nAg through Cl^- and biomolecules. Additionally, we showed that the stability of the formed nAg was controlled by both 0-3 kDa and >3 kDa fraction. The nAg formation dynamics and mechanism unraveled in this study will further our knowledge on the biochemical conversions among Ag^+, AgCl, and nAg and assist in future evaluation of their behavior and fate in the environment and biota.

Conflicts of interest

There are no conflicts to declare.

Acknowledgements

The authors acknowledge the financial support by USDA NIFA Hatch Program (MAS00549), USDA-NIFA (2015-67017-23070), and BARD (IS-4964-16R) for this work. Huiyuan is also thankful for the Lotta Crabtree Fellowship provided by the Lotta Crabtree Fund.

Supporting information

Additional information is available in the supporting information: sample preparation, characterization methods, and the resulting figures for SEM-EDS, HRTEM, SAED, SERS, and FTIR; DLS characterization of the formed particles by light-irradiated pristine RE; UV-Vis absorbance spectra of pristine RE, formation of nAg as influenced by RE boiling, purge, addition of SOD or Na^+; transformation kinetics regression; and GC-MS analysis of RE composition.

References

(1) Yin, Y.; Liu, J.; Jiang, G. Sunlight-induced reduction of ionic Ag and Au to metallic nanoparticles by dissolved organic matter. *ACS Nano* **2012**, *6* (9), 7910–7919.

(2) Yin, Y.; Shen, M.; Zhou, X.; Yu, S.; Chao, J.; Liu, J.; Jiang, G. Photoreduction and Stabilization Capability of Molecular Weight Fractionated Natural Organic Matter in Transformation of Silver Ion to Metallic Nanoparticle. *Environ. Sci. Technol.* **2014**, *48* (16), 9366–9373.

(3) Hou, W.; Stuart, B.; Zepp, R. G. Sunlight drive reduction of silver ion by natural organic matter: Formation and transformation of silver nanoparticles. *Environ. Sci. Technol.* **2013**, *47*, 7713–7721.

(4) Kang, F.; Alvarez, P. J.; Zhu, D. Microbial Extracellular Polymeric Substances Reduce Ag+ to Silver Nanoparticles and Antagonize Bactericidal Activity. *Environ. Sci. Technol.* **2014**, *48* (1), 316–322.

(5) Pardha-Saradhi, P.; Yamal, G.; Peddisetty, T.; Sharmila, P.; Nagar, S.; Singh, J.; Nagarajan, R.; Rao, K. S. Reducing Strength Prevailing at Root Surface of Plants Promotes Reduction of Ag+ and Generation of Ag0/Ag2O Nanoparticles Exogenously in Aqueous Phase. *PLoS One* **2014**, *9* (9), 1–13.

(6) Shabnam, N.; Sharmila, P.; Govindjee; Kim, H.; Pardha-Saradhi, P. Differential Response

of Floating and Submerged Leaves of Longleaf Pondweed to Silver Ions. *Front. Plant Sci.* **2017**, *8*, 1–14.

(7) Shabnam, N.; Sharmila, P.; Kim, H.; Pardha-Saradhi, P. Light mediated generation of silver nanoparticles by spinach thylakoids/chloroplasts. *PLoS One* **2016**, *11* (12), 1–13.

(8) Beattie, I. R.; Haverkamp, R. G. Silver and gold nanoparticles in plants: sites for the reduction to metal. *Metallomics* **2011**, *3* (6), 628.

(9) Gardea-Torresdey, J. L.; Gomez, E.; Peralta-Videa, J. R.; Parsons, J. G.; Troiani, H.; Jose-Yacaman, M. Alfalfa sprouts: A natural source for the synthesis of silver nanoparticles. *Langmuir* **2003**, *19* (4), 1357–1361.

(10) Guo, H.; Ma, C.; Thistle, L.; Huynh, M.; Yu, C.; Clasby, D.; Chefetz, B.; Polubesova, T.; White, J. C.; He, L.; et al. Transformation of Ag ions into Ag nanoparticle-loaded AgCl microcubes in the plant root zone. *Environ. Sci. Nano* **2019**, *6* (4), 1099–1110.

(11) Lisec, J.; Schauer, N.; Kopka, J.; Willmitzer, L.; Fernie, A. R. Gas chromatography mass spectrometry-based metabolite profiling in plants. *Nat. Protoc.* **2006**, *1* (1), 387–396.

(12) Evans, L. J.; Barabash, S. J. Molybdenum, Silver, Thallium and Vanadium. In *Trace Elements in Soils*; John Wiley & Sons, Ltd: Chichester, UK, 2010; pp 515–549.

(13) Purcell, T. W.; Peters, J. J. Sources of silver in the environment. *Environ. Toxicol. Chem.* **1998**, *17* (4), 539–546.

(14) Wijnhoven, S. W. P.; Peijnenburg, W. J. G. M.; Herberts, C. a; Hagens, W. I.; Oomen, A. G.; Heugens, E. H. W.; Roszek, B.; Bisschops, J.; Gosens, I.; Van De Meent, D.; et al. Nano-silver – a review of available data and knowledge gaps in human and environmental risk assessment. *Nanotoxicology* **2009**, *3* (2), 109–138.

(15) Howe, P. D.; Dobson, S. Silver and silver compounds: Environmental aspects. *IPCS Concise Int. Chem. Assess. Doc.* **2002**, 1–36.

(16) Guo, H.; Zhang, Z.; Xing, B.; Mukherjee, A.; Musante, C.; White, J. C.; He, L. Analysis of Silver Nanoparticles in Antimicrobial Products Using Surface-Enhanced Raman Spectroscopy (SERS). *Environ. Sci. Technol.* **2015**, *49* (7), 4317–4324.

(17) Yin, Y.; Xu, W.; Tan, Z.; Li, Y.; Wang, W.; Guo, X.; Yu, S.; Liu, J.; Jiang, G. Photo- and thermo-chemical transformation of AgCl and Ag2S in environmental matrices and its implication. *Environ. Pollut.* **2017**, *220*, 955–962.

(18) Scopes, R. K. Measurement of protein by spectrophotometry at 205 nm. *Anal. Biochem.* **1974**, *59* (1), 277–282.

(19) Adegboyega, N. F.; Sharma, V. K.; Siskova, K.; Zbořil, R.; Sohn, M.; Schultz, B. J.; Banerjee, S. Interactions of Aqueous Ag+ with Fulvic Acids: Mechanisms of Silver Nanoparticle Formation and Investigation of Stability. *Environ. Sci. Technol.* **2013**, *47* (2), 757–764.

(20) Zhang, X.; Yang, C.-W.; Yu, H.-Q.; Sheng, G.-P. Light-induced reduction of silver ions to silver nanoparticles in aquatic environments by microbial extracellular polymeric substances (EPS). *Water Res.* **2016**, *106*, 242–248.

(21) Guo, H.; He, L.; Xing, B. Applications of surface-enhanced Raman spectroscopy in the

analysis of nanoparticles in the environment. *Environ. Sci. Nano* **2017**, *4*, 2093–2107.

(22) Wei, H.; Hossein Abtahi, S. M.; Vikesland, P. J. Plasmonic colorimetric and SERS sensors for environmental analysis. *Environ. Sci. Nano* **2015**, *2* (2), 120–135.

(23) Chulovskaya, S. a.; Garas'ko, E. V.; Parfenyuk, V. I. Electrochemical preparation and properties of ultradisperce silver powder. *Russ. J. Appl. Chem.* **2009**, *82* (8), 1396–1400.

(24) Bogdanchikova, N.; Meunier, F. C.; Avalos-Borja, M.; Breen, J. P.; Pestryakov, A. On the nature of the silver phases of Ag/Al2O3 catalysts for reactions involving nitric oxide. *Appl. Catal. B-Environmental* **2002**, *36* (4), 287–297.

(25) Jones, A. M.; Garg, S.; He, D.; Pham, A. N.; Waite, T. D. Superoxide-mediated formation and charging of silver nanoparticles. *Environ. Sci. Technol.* **2011**, *45* (4), 1428–1434.

(26) Lambert, J. B. *Introduction to organic spectroscopy.*; New York: Macmillan, 1987.

(27) Larkin, P. J. *IR and Raman Spectroscopy - Principles and Spectral Interpretation*, 1st ed.; Elsevier, 2011.

(28) Sánchez-Cortés, S.; García-Ramos, J. V. SERS of AMP on different silver colloids. *J. Mol. Struct.* **1992**, *274* (C), 33–45.

(29) Li, Y. S.; Cheng, J.; Wang, Y. Surface-enhanced Raman spectra of dyes and organic acids in silver solutions: Chloride ion effect. *Spectrochim. Acta - Part A Mol. Biomol. Spectrosc.* **2000**, *56* (11), 2067–2072.

(30) Peterson, K. I.; Lipnick, M. E.; Mejia, L. A.; Pullman, D. P. Temperature Dependence and Mechanism of Chloride-Induced Aggregation of Silver Nanoparticles. *J. Phys. Chem. C* **2016**, *120*, 23268–23275.

(31) Sharma, M.; Das, B.; Sarmah, J. C.; Hazarika, A.; Deka, B. K.; Park, Y.; Bania, K. K. Fractal to monolayer growth of AgCl and Ag/AgCl. *J. Mater. Chem. A Mater. energy Sustain.* **2017**, *00*, 1–11.

(32) Rasulov, B. A.; Davranov, K. D.; Wen, L. Formation of Ag/AgCl Nanoparticles in the Matrix of the Exopolysaccharide of a Diazotrophic Strain Azotobacter chroococcum XU1. *Microbiology* **2017**, *86* (2), 182–187.

(33) Liu, H.; Gu, X.; Wei, C.; Fu, H.; Alvarez, P. J. J.; Li, Q.; Zheng, S.; Qu, X.; Zhu, D. Threshold Concentrations of Silver Ions Exist for the Sunlight-Induced Formation of Silver Nanoparticles in the Presence of Natural Organic Matter. *Environ. Sci. Technol.* **2018**, acs.est.7b05645.

(34) Kracht, S.; Messerer, M.; Lang, M.; Eckhardt, S.; Lauz, M.; Grobéty, B.; Fromm, K. M.; Giese, B. Electron transfer in peptides: On the formation of silver nanoparticles. *Angew. Chemie - Int. Ed.* **2015**, *54* (10), 2912–2916.

(35) Sumi, S.; Watanabe, T.; Fujishima, A.; Honda, K. Effect of Cl− and Br− Ions and pH on the Flatband Potentials of Silver Halide Sheet Crystal Electrodes. *Bull. Chem. Soc. Jpn.* **2006**, *53* (10), 2742–2747.

(36) Glaus, S.; Calzaferri, G. The band structures of the silver halides AgF, AgCl, and AgBr: A comparative study. *Photochem. Photobiol. Sci.* **2003**, *2* (4), 398.

(37) Glaus, S.; Calzaferri, G.; Hoffmann, R. Electronic Properties of the Silver–Silver Chloride Cluster Interface. *Chem. - A Eur. J.* **2002**, *8* (8), 1785.

(38) Daupor, H.; Chenea, A. Degradation of blue and red inks by Ag/AgCl photocatalyst under UV light irradiation. In *AIP Conference Proceedings*; 2017; Vol. 1868, p 020009.

(39) Lanz, M.; Schürch, D.; Calzaferri, G. Photocatalytic oxidation of water to O2 on AgCl-coated electrodes. *J. Photochem. Photobiol. A Chem.* **1999**, *120* (2), 105–117.

(40) Currao, A.; Reddy, V. R.; Calzaferri, G. Gold-Colloid-Modified AgCl Photocatalyst for Water Oxidation to O2. *ChemPhysChem* **2004**, *5* (5), 720–724.

(41) Song, J.; Roh, J.; Lee, I.; Jang, J. Low temperature aqueous phase synthesis of silver/silver chloride plasmonic nanoparticles as visible light photocatalysts. *Dalt. Trans.* **2013**, *42* (38), 13897.

(42) Wang, G.; Nishio, T.; Sato, M.; Ishikawa, A.; Nambara, K.; Nagakawa, K.; Matsuo, Y.; Niikura, K.; Ijiro, K. Inspiration from chemical photography: accelerated photoconversion of AgCl to functional silver nanoparticles mediated by DNA. *Chem. Commun.* **2011**, *47* (33), 9426.

(43) Wang, P.; Huang, B.; Qin, X.; Zhang, X.; Dai, Y.; Wei, J.; Whangbo, M.-H. Ag@AgCl: A Highly Efficient and Stable Photocatalyst Active under Visible Light. *Angew. Chemie Int. Ed.* **2008**, *47* (41), 7931–7933.

(44) Garg, S.; Rong, H.; Miller, C. J.; Waite, T. D. Chlorine-Mediated Regeneration of Semiconducting AgCl(s) Following Light-Induced Ag0 Formation: Implications to Contaminant Degradation. *J. Phys. Chem. C* **2016**, *120* (11), 5988–5996.

(45) White, P. J.; Broadley, M. R. Chloride in soils and its uptake and movement within the plant: A review. *Ann. Bot.* **2001**, *88* (6), 967–988.

(46) Guo, X.; Yin, Y.; Tan, Z.; Liu, J. Environmentally Relevant Freeze-Thaw Cycles Enhance the Redox-Mediated Morphological Changes of Silver Nanoparticles. *Environ. Sci. Technol.* **2018**, *52* (12), 6928–6935.

(47) Li, S.; Shen, Y.; Xie, A.; Yu, X.; Qiu, L.; Zhang, L.; Zhang, Q. Green synthesis of silver nanoparticles using Capsicum annuum L. extract. *Green Chem.* **2007**, *9* (8), 852.

(48) Siciliano, S. D.; Goldie, H.; Germida, J. J. Enzymatic activity in root exudates of Dahurian wild rye (Elymus dauricus) that degrades 2-chlorobenzoic acid. *J. Agric. Food Chem.* **1998**, *46* (1), 5–7.

(49) Wang, P.; Bi, S.; Wang, S.; Ding, Q. Variation of wheat root exudates under aluminum stress. *J. Agric. Food Chem.* **2006**, *54* (26), 10040–10046.

(50) Nóbrega, F. M.; Santos, I. S.; Da Cunha, M.; Carvalho, A. O.; Gomes, V. M. Antimicrobial proteins from cowpea root exudates: Inhibitory activity against Fusarium oxysporum and purification of a chitinase-like protein. *Plant Soil* **2005**, *272* (1–2), 223–232.

(51) Talekar, S.; Joshi, A.; Chougle, R.; Nakhe, A.; Bhojwani, R. Immobilized enzyme mediated synthesis of silver nanoparticles using cross-linked enzyme aggregates (CLEAs) of NADH-dependent nitrate reductase. *Nano-Structures & Nano-Objects* **2016**, *6*, 23–33.

(52) Hebbalalu, D.; Lalley, J.; Nadagouda, M. N.; Varma, R. S. Greener techniques for the

synthesis of silver nanoparticles using plant extracts, enzymes, bacteria, biodegradable polymers, and microwaves. *ACS Sustain. Chem. Eng.* **2013**, *1* (7), 703–712.

(53) Naik, R. R.; Stringer, S. J.; Agarwal, G.; Jones, S. E.; Stone, M. O. Biomimetic synthesis and patterning of silver nanoparticles. *Nat. Mater.* **2002**, *1* (3), 169–172.

(54) Yin, X.; Chen, S.; Wu, A. Green chemistry synthesis of gold nanoparticles using lactic acid as a reducing agent. *Micro Nano Lett.* **2010**, *5* (5), 270.

(55) Pettegrew, C.; Dong, Z.; Muhi, M. Z.; Pease, S.; Mottaleb, M. A.; Islam, M. R. Silver Nanoparticle Synthesis Using Monosaccharides and Their Growth Inhibitory Activity against Gram-Negative and Positive Bacteria. *ISRN Nanotechnol.* **2014**, *2014*, 1–8.

(56) El-Rafie, M. H.; Ahmed, H. B.; Zahran, M. K. Facile Precursor for Synthesis of Silver Nanoparticles Using Alkali Treated Maize Starch. *Int. Sch. Res. Not.* **2014**, *2014*, 1–12.

(57) Suresh, A. K.; Pelletier, D. A.; Wang, W.; Moon, J.-W.; Gu, B.; Mortensen, N. P.; Allison, D. P.; Joy, D. C.; Phelps, T. J.; Doktycz, M. J. Silver Nanocrystallites: Biofabrication using *Shewanella oneidensis,* and an Evaluation of Their Comparative Toxicity on Gram-negative and Gram-positive Bacteria. *Environ. Sci. Technol.* **2010**, *44* (13), 5210–5215.

(58) Eckhardt, S.; Brunetto, P. S.; Gagnon, J.; Priebe, M.; Giese, B.; Fromm, K. M. Nanobio silver: Its interactions with peptides and bacteria, and its uses in medicine. *Chem. Rev.* **2013**, *113* (7), 4708–4754.

(59) Hou, W.; Stuart, B.; Howes, R.; Zepp, R. G. Sunlight-Driven Reduction of Silver Ions by Natural Organic Matter: Formation and Transformation of Silver Nanoparticles. *Environ. Sci. Technol.* **2013**, *47* (14), 7713–7721.

(60) Huynh, K. A.; Chen, K. L. Aggregation kinetics of citrate and polyvinylpyrrolidone coated silver nanoparticles in monovalent and divalent electrolyte solutions. *Environ. Sci. Technol.* **2011**, *45* (13), 5564–5571.

(61) Baalousha, M.; Nur, Y.; Römer, I.; Tejamaya, M.; Lead, J. R. Effect of monovalent and divalent cations, anions and fulvic acid on aggregation of citrate-coated silver nanoparticles. *Sci. Total Environ.* **2013**, *454–455*, 119–131.

(62) Li, X.; Lenhart, J. J.; Walker, H. W. Dissolution-accompanied aggregation kinetics of silver nanoparticles. *Langmuir* **2010**, *26* (22), 16690–16698.

(63) Prütz, W. A. Hypochlorous acid interactions with thiols, nucleotides, DNA, and other biological substrates. *Arch. Biochem. Biophys.* **1996**, *332* (1), 110–120.

(64) Hazen, S. L.; D'Avignon, A.; Anderson, M. M.; Hsu, F. F.; Heinecke, J. W. Human neutrophils employ the myeloperoxidase-hydrogen peroxide-chloride system to oxidize α-amino acids to a family of reactive aldehydes: Mechanistic studies identifying labile intermediates along the reaction pathway. *J. Biol. Chem.* **1998**, *273* (9), 4997–5005.

(65) Prütz, W. A. Interactions of hypochlorous acid with pyrimidine nucleotides, and secondary reactions of chlorinated pyrimidines with GSH, NADH, and other substrates. *Arch. Biochem. Biophys.* **1998**, *349* (1), 183–191.

(66) Singh, A.; Hou, W. C.; Lin, T. F.; Zepp, R. G. Roles of Silver-Chloride Complexations in Sunlight-Driven Formation of Silver Nanoparticles. *Environ. Sci. Technol.* **2019**.

(67) Hebert, V. R.; Miller, G. C. Depth Dependence of Direct and Indirect Photolysis on Soil Surfaces. *J. Agric. Food Chem.* **1990**, *38* (3), 913–918.

(68) Pearsall, B. W. H.; Ullyott, P. Light Penetration Into Fresh Water: I. a Thermionic Potentiometer for Measuring Light Intensity With Photo-Electric Cells. *J. Exp. Biol.* **1933**, *10* (4), 293–305.

(69) Adegboyega, N. F.; Sharma, V. K.; Siskova, K. M.; Vecerova, R.; Kolar, M.; Zbořil, R.; Gardea-Torresdey, J. L. Enhanced formation of silver nanoparticles in Ag+-NOM-iron(II, III) systems and antibacterial activity studies. *Environ. Sci. Technol.* **2014**, *48* (6), 3228–3235.

(70) Zhang, X.; Yang, C. W.; Yu, H. Q.; Sheng, G. P. Light-induced reduction of silver ions to silver nanoparticles in aquatic environments by microbial extracellular polymeric substances (EPS). *Water Res.* **2016**, *106*, 242–248.

(71) Levard, C.; Hotze, E. M.; Lowry, G. V.; Brown, G. E. Environmental transformations of silver nanoparticles: Impact on stability and toxicity. *Environ. Sci. Technol.* **2012**, *46* (13), 6900–6914.

(72) Sharma, V. K.; Filip, J.; Zboril, R.; Varma, R. S. Natural inorganic nanoparticles - formation, fate, and toxicity in the environment. *Chem. Soc. Rev.* **2015**, *44*, 8410–8423.

(73) Li, L.; Zhou, Q.; Geng, F.; Wang, Y.; Jiang, G. Formation of Nanosilver from Silver Sulfide Nanoparticles in Natural Waters by Photoinduced Fe(II, III) Redox Cycling. *Environ. Sci. Technol.* **2016**, *50*, 13342−13350.

Figures

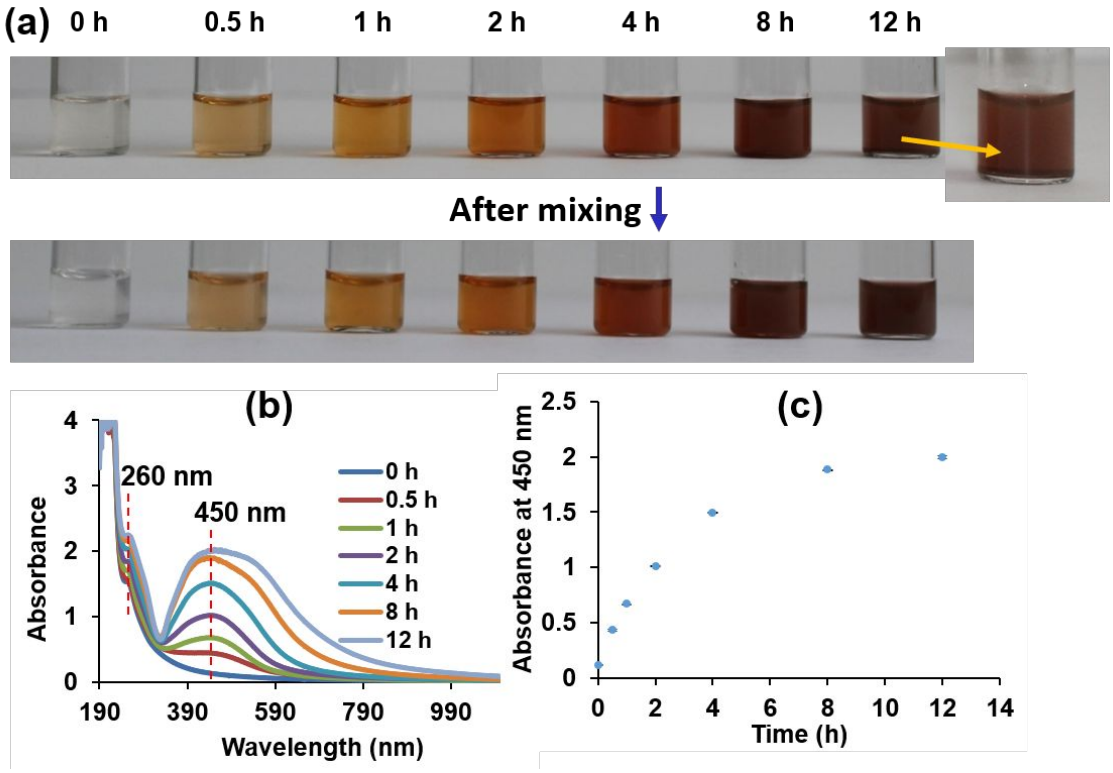

Figure 1. Sample color change over time (0-12 h) (a) and the corresponding UV-Vis spectra (b) demonstrate the formation of nAg in the presence of Ag^+ (1 mM) and RE. The sample solutions were well mixed before recording the UV-Vis absorbance. The characteristic peak of nAg at 450 nm was used to track the dynamics of nAg formation (c).

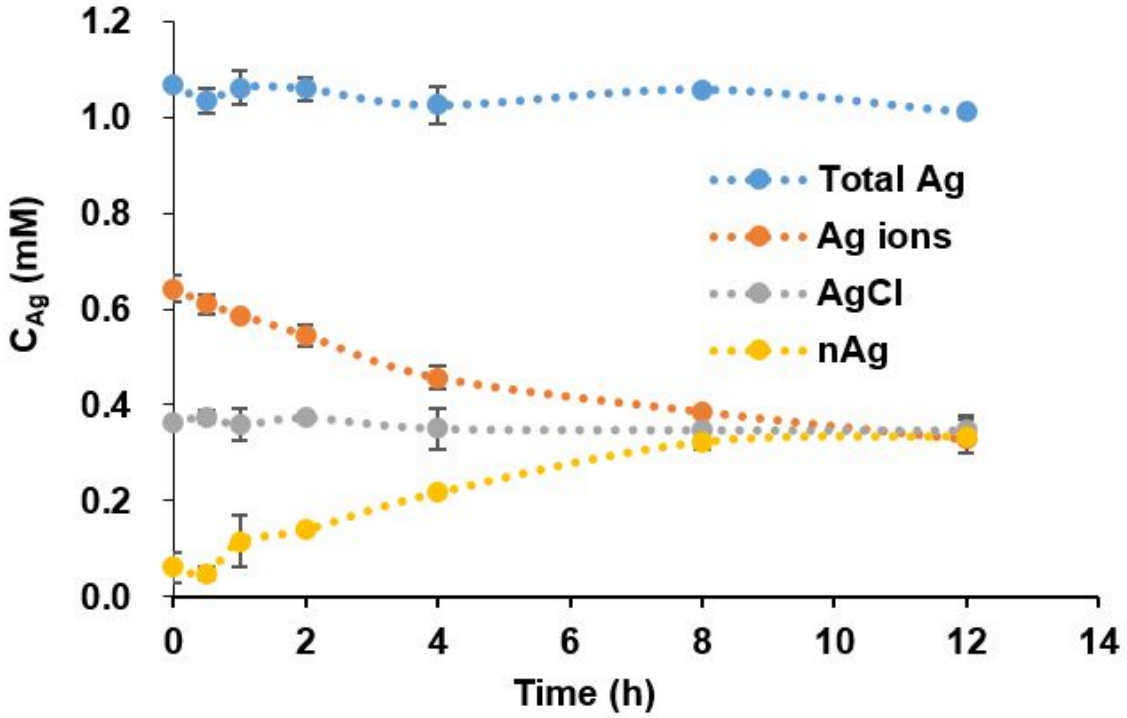

Figure 2. Quantification of the silver species (Ag^+, AgCl, and nAg) by ICP-MS after separation at different time points (0-12 h) during the photo-induced transformation of Ag^+ by RE.

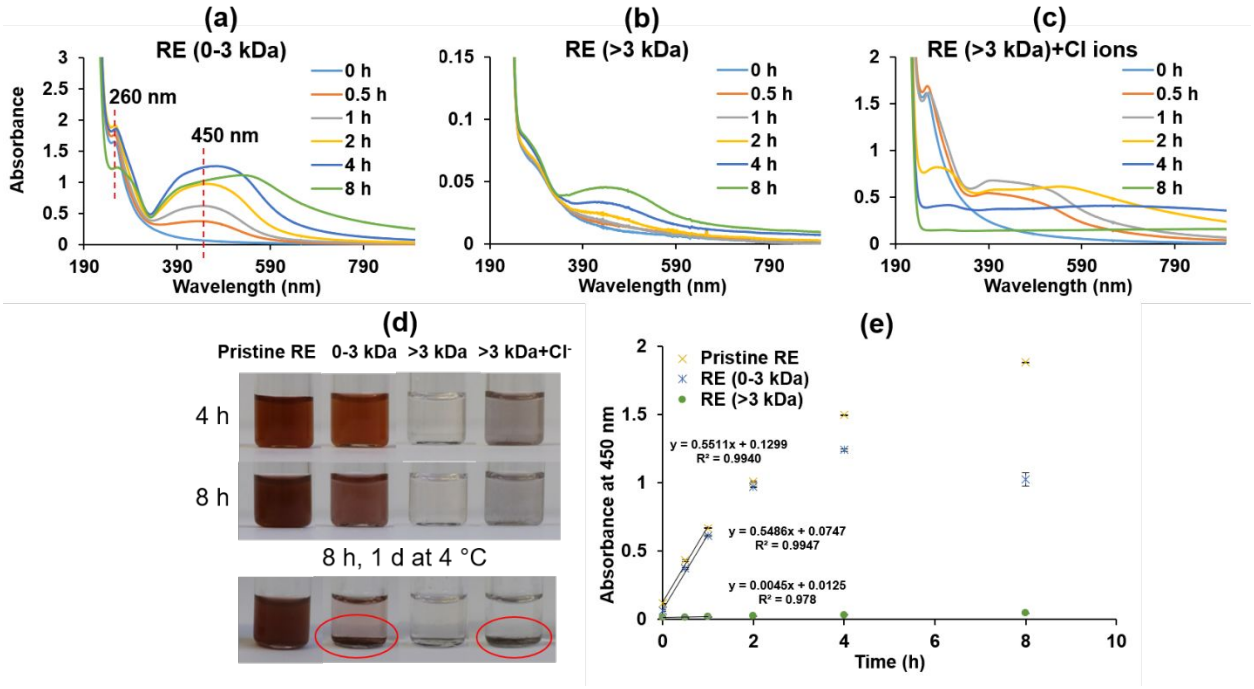

Figure 3. Interaction of Ag^+ (1 mM) with different fractions of RE (molecular weight-based) under light exposure: (a) 0-3 kDa, and (b) >3 kDa. In order to test the effect of Cl^-, additional Cl^- (0.33 mM) were added into RE (>3 kDa) (c). The appearances of suspensions at 4 h, 8 h and after 1 d storage of the 8 h sample at 4 °C were shown in (d). The samples at different time points were well mixed prior to UV-Vis absorbance analysis. The nAg formation kinetics were depicted in (e) based on the UV-Vis absorbance at 450 nm. As the spectral pattern in (c) is different from those in (a) and (b), it is not included in (e).

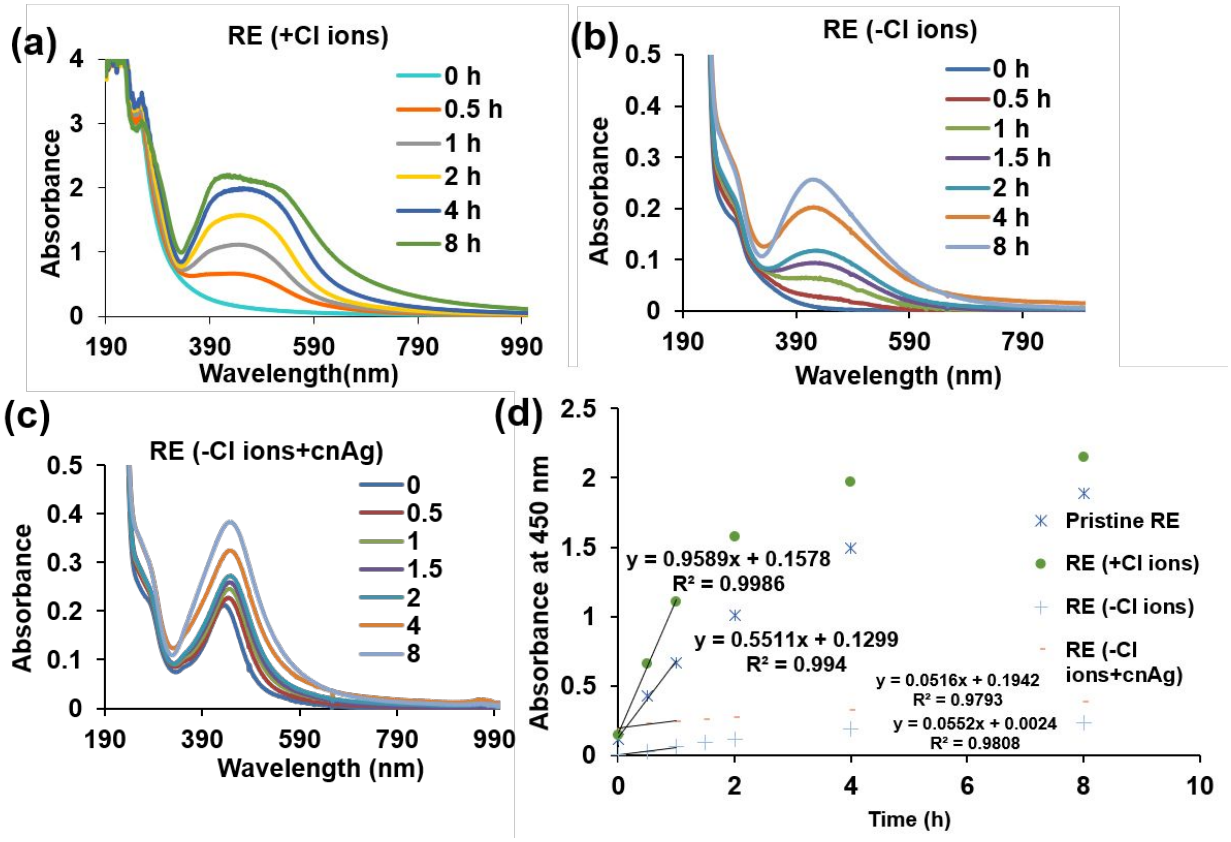

Figure 4. UV-Vis absorbance spectra of the formed nAg by RE after adding additional 0.33 mM Cl^- (a), removing original Cl^- (b), or removing Cl^- and adding citrate-coated nAg (1 mg/L) as seeds (c). The initial formation rate (0-1 h) (d) was calculated based on UV-Vis absorbance at 450 nm and compared among three treatments and pristine RE.

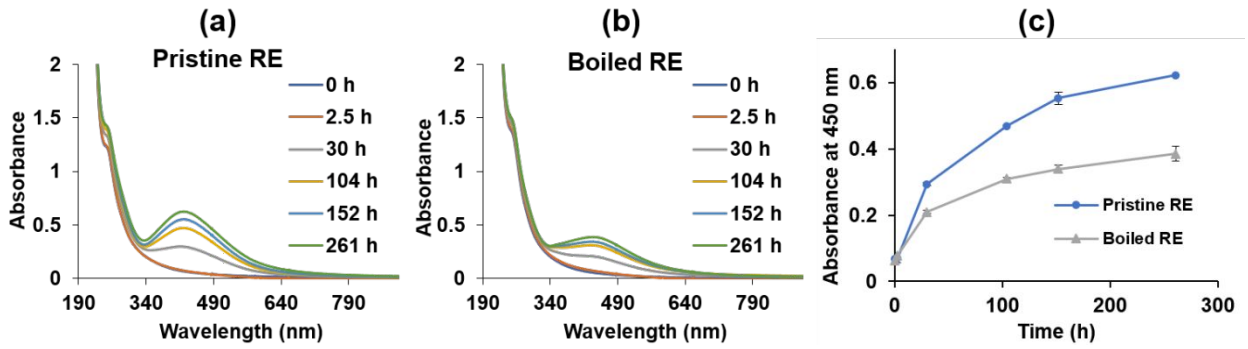

Figure 5. Transformation of Ag^+ (1 mM) by pristine (a) and boiled RE (b) in the dark. The UV-Vis absorbance at 450 nm was recorded to demonstrate the nAg formation dynamics (c). Lines were made based on eyes and used to show the general trend of the transformation.

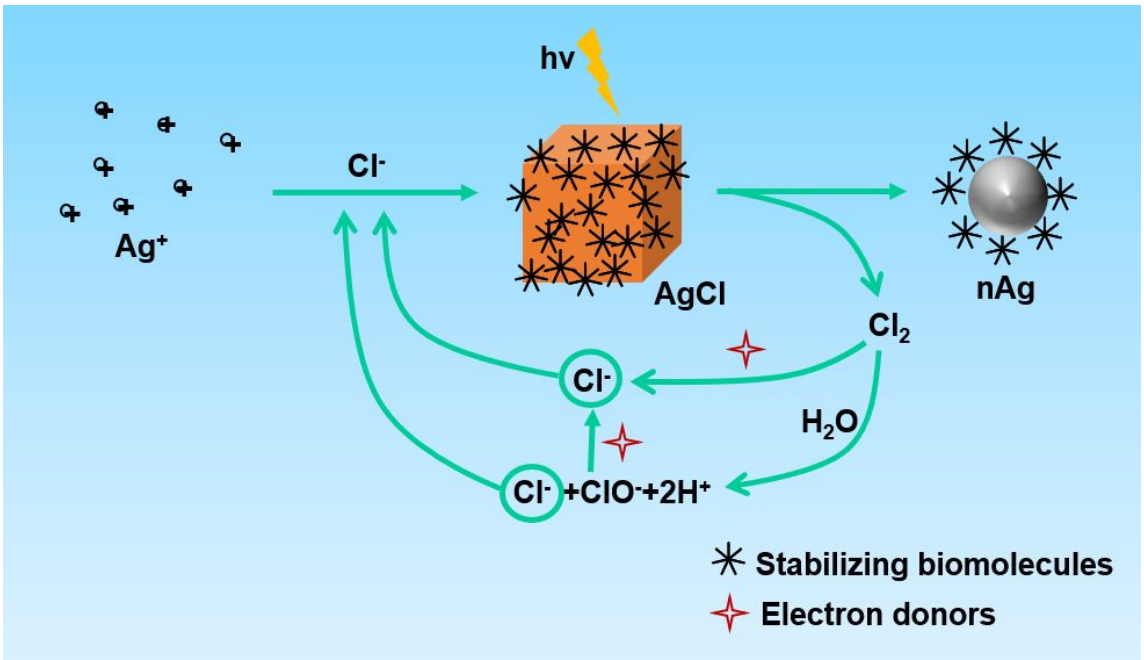

Figure 6. Schematic illustration of the mechanisms underlying photo-induced Ag^+ transformation in root exudates.